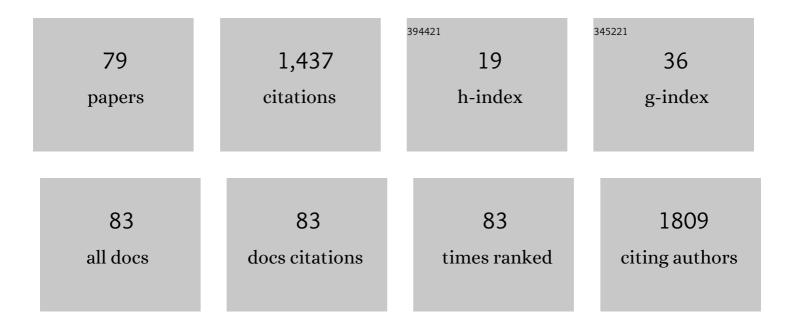
List of Publications by Year in descending order

Source: https://exaly.com/author-pdf/422889/publications.pdf Version: 2024-02-01



WENLL CA

#	Article	IF	CITATIONS
1	Quantitative Assessment of Whole-Body Tumor Burden in Adult Patients with Neurofibromatosis. PLoS ONE, 2012, 7, e35711.	2.5	126
2	Diagnostic Accuracy of Laxative-Free Computed Tomographic Colonography for Detection of Adenomatous Polyps in Asymptomatic Adults. Annals of Internal Medicine, 2012, 156, 692.	3.9	103
3	Data Intermixing and Multi-volume Rendering. Computer Graphics Forum, 1999, 18, 359-368.	3.0	102
4	Tumor Burden in Patients with Neurofibromatosis Types 1 and 2 and Schwannomatosis: Determination on Whole-Body MR Images. Radiology, 2009, 250, 665-673.	7.3	102
5	CT Quantification and Machine-learning Models for Assessment of Disease Severity and Prognosis of COVID-19 Patients. Academic Radiology, 2020, 27, 1665-1678.	2.5	74
6	Predicting the response to neoadjuvant chemotherapy for breast cancer: wavelet transforming radiomics in MRI. BMC Cancer, 2020, 20, 100.	2.6	68
7	Current whole-body MRI applications in the neurofibromatoses. Neurology, 2016, 87, S31-9.	1.1	65
8	Benign whole body tumor volume is a risk factor for malignant peripheral nerve sheath tumors in neurofibromatosis type 1. Journal of Neuro-Oncology, 2014, 116, 307-313.	2.9	59
9	Structure-analysis method for electronic cleansing in cathartic and noncathartic CT colonography. Medical Physics, 2008, 35, 3259-3277.	3.0	49
10	Measurement of Glenoid Bone Loss With 3-Dimensional Magnetic Resonance Imaging: A Matched Computed Tomography Analysis. Arthroscopy - Journal of Arthroscopic and Related Surgery, 2018, 34, 3141-3147.	2.7	43
11	Relationship between wholeâ€body tumor burden, clinical phenotype, and quality of life in patients with neurofibromatosis. American Journal of Medical Genetics, Part A, 2014, 164, 1431-1437.	1.2	41
12	The metastatic promoter DEPDC1B induces epithelialâ€mesenchymal transition and promotes prostate cancer cell proliferation via Rac1â€PAK1 signaling. Clinical and Translational Medicine, 2020, 10, e191.	4.0	37
13	Diagnostic Value of Gadoxetic Acid-Enhanced MR Imaging to Distinguish HCA and Its Subtype from FNH: A Systematic Review. International Journal of Medical Sciences, 2017, 14, 668-674.	2.5	34
14	Informatics in Radiology: Dual-Energy Electronic Cleansing for Fecal-Tagging CT Colonography. Radiographics, 2013, 33, 891-912.	3.3	31
15	MDCT for Automated Detection and Measurement of Pneumothoraces in Trauma Patients. American Journal of Roentgenology, 2009, 192, 830-836.	2.2	28
16	Informatics in Radiology: Electronic Cleansing for Noncathartic CT Colonography: A Structure-Analysis Scheme. Radiographics, 2010, 30, 585-602.	3.3	28
17	Dynamic-Threshold Level Set Method for Volumetry of Porcine Kidney in CT Images. Academic Radiology, 2007, 14, 890-896.	2.5	27
18	Mosaic Decomposition: An Electronic Cleansing Method for Inhomogeneously Tagged Regions in Noncathartic CT Colonography. IEEE Transactions on Medical Imaging, 2011, 30, 559-574.	8.9	25

#	Article	IF	CITATIONS
19	Maximum Intensity Projection Using Splatting in Sheared Object Space. Computer Graphics Forum, 1998, 17, 113-124.	3.0	22
20	Comparative Evaluation of the Fecal-Tagging Quality in CT Colonography. Academic Radiology, 2009, 16, 1393-1399.	2.5	21
21	Pain correlates with germline mutation in schwannomatosis. Medicine (United States), 2018, 97, e9717.	1.0	20
22	MDCT quantification is the dominant parameter in decision-making regarding chest tube drainage for stable patients with traumatic pneumothorax. Computerized Medical Imaging and Graphics, 2012, 36, 375-386.	5.8	19
23	Diagnostic Value of Multidetector CT and Its Multiplanar Reformation, Volume Rendering and Virtual Bronchoscopy Postprocessing Techniques for Primary Trachea and Main Bronchus Tumors. PLoS ONE, 2015, 10, e0137329.	2.5	19
24	Diagnostic Value of Gd-EOB-DTPA-MRI for Hepatocellular Adenoma: A Meta-Analysis. Journal of Cancer, 2017, 8, 1301-1310.	2.5	18
25	Volumetric MRI Analysis of Plexiform Neurofibromas in Neurofibromatosis Type 1. Academic Radiology, 2018, 25, 144-152.	2.5	17
26	Immune Cytolytic Activity as an Indicator of Immune Checkpoint Inhibitors Treatment for Prostate Cancer. Frontiers in Bioengineering and Biotechnology, 2020, 8, 930.	4.1	17
27	Quantitative image analysis for evaluation of tumor response in clinical oncology. Chronic Diseases and Translational Medicine, 2018, 4, 18-28.	1.2	16
28	B7 score and T cell infiltration stratify immune status in prostate cancer. , 2021, 9, e002455.		16
29	MDCT for Computerized Volumetry of Pneumothoraces in Pediatric Patients. Academic Radiology, 2011, 18, 315-323.	2.5	14
30	Collaborative Virtual Simulation Environment for Radiotherapy Treatment Planning. Computer Graphics Forum, 2000, 19, 379-390.	3.0	13
31	Electronic Cleansing in Fecal-Tagging Dual-Energy CT Colonography Based on Material Decomposition and Virtual Colon Tagging. IEEE Transactions on Biomedical Engineering, 2015, 62, 754-765.	4.2	12
32	Correlation between NF1 genotype and imaging phenotype on whole-body MRI. Neurology, 2020, 94, e2521-e2531.	1.1	12
33	Risk stratification of thymic epithelial tumors by using a nomogram combined with radiomic features and TNM staging. European Radiology, 2021, 31, 423-435.	4.5	12
34	Loss of NEIL3 activates radiotherapy resistance in the progression of prostate cancer. Cancer Biology and Medicine, 2022, 19, 1193-1210.	3.0	12
35	Influence of feature calculating parameters on the reproducibility of CT radiomic features: a thoracic phantom study. Quantitative Imaging in Medicine and Surgery, 2020, 10, 1775-1785.	2.0	11
36	Dual-Energy Index Value of Luminal Air in Fecal-Tagging Computed Tomography Colonography. Journal of Computer Assisted Tomography, 2013, 37, 183-194.	0.9	10

#	Article	IF	CITATIONS
37	Deep Parametric Active Contour Model for Neurofibromatosis Segmentation. Future Generation Computer Systems, 2020, 112, 58-66.	7.5	10
38	Image Quality and Radiation Dose of CT Coronary Angiography with Automatic Tube Current Modulation and Strong Adaptive Iterative Dose Reduction Three-Dimensional (AIDR3D). PLoS ONE, 2015, 10, e0142185.	2.5	9
39	Iterative mesh transformation for 3D segmentation of livers with cancers in CT images. Computerized Medical Imaging and Graphics, 2015, 43, 1-14.	5.8	9
40	Radiomics Analysis of Gd-EOB-DTPA Enhanced Hepatic MRI for Assessment of Functional Liver Reserve. Academic Radiology, 2022, 29, 213-218.	2.5	8
41	Minimum-invasive early diagnosis of colorectal cancer with CT colonography: techniques and clinical value. Expert Opinion on Medical Diagnostics, 2008, 2, 1233-1246.	1.6	6
42	Scalable, high-performance 3D imaging software platform: System architecture and application to virtual colonoscopy. , 2012, 2012, 3994-7.		6
43	Topoisomerase II-binding protein 1 promotes the progression of prostate cancer via ATR-CHK1 signaling pathway. Aging, 2020, 12, 9948-9958.	3.1	6
44	Digital bowel cleansing for computer-aided detection of polyps in fecal-tagging CT colonography. , 2006, , .		5
45	Delineation of tagged region by use of local iso-surface roughness in electronic cleansing for CT colonography. , 2007, , .		5
46	Plasma S100β is not a useful biomarker for tumor burden in neurofibromatosis. Clinical Biochemistry, 2013, 46, 698-700.	1.9	5
47	3D planar reformation of vascular central axis surface with biconvex slab. Computerized Medical Imaging and Graphics, 2007, 31, 570-576.	5.8	4
48	Fecal-tagging CT colonography with structure-analysis electronic cleansing for detection of colorectal flat lesions. European Journal of Radiology, 2012, 81, 1712-1716.	2.6	4
49	Use of multidetector computed tomography to guide management of pneumothorax. Current Opinion in Pulmonary Medicine, 2013, 19, 387-393.	2.6	4
50	COMPUTATION OF VESSELNESS IN CTA IMAGES FOR FAST AND INTERACTIVE VESSEL SEGMENTATION. International Journal of Image and Graphics, 2007, 07, 159-176.	1.5	3
51	Pseudo-enhancement correction for computer-aided detection in fecal-tagging CT colonography. , 2007, , .		3
52	Virtual colon tagging for electronic cleansing in dual-energy fecal-tagging CT colonography. , 2012, 2012, 3736-9.		3
53	A comparative study of effective atomic number calculations for dualâ€energy CT. Medical Physics, 2021, 48, 5908-5923.	3.0	3
54	Role of 3D Volumetric and Perfusion Imaging for Detecting Early Changes in Pancreatic Adenocarcinoma. Frontiers in Oncology, 2021, 11, 678617.	2.8	3

#	Article	IF	CITATIONS
55	A Low-Cost Highly Configurable Phantom for Simulation of Imaging-Guided Endocavitary Procedures. Ultrasound Quarterly, 2019, 35, 61-67.	0.8	2
56	Tracer Kinetic Modeling by Morales-Smith Hypothesis in Hepatic Perfusion CT. Lecture Notes in Computer Science, 2012, , 292-302.	1.3	2
57	Vesselness propagation: a fast interactive vessel segmentation method. , 2006, , .		1
58	Mosaic decomposition method for detection and removal of inhomogeneously tagged regions in electronic cleansing for CT colonography. Proceedings of SPIE, 2008, , .	0.8	1
59	Computer-aided detection of polyps in CT colonography: Performance evaluation in comparison with human readers based on large multicenter clinical trial cases. , 2009, , .		1
60	Dual-energy electronic cleansing for non-cathartic CT colonography: a phantom study. Proceedings of SPIE, 2010, , .	0.8	1
61	Low-dose dual-energy electronic cleansing for fecal-tagging CT Colonography. , 2013, , .		1
62	Pilot Study on Image Quality and Radiation Dose of CT Colonography with Adaptive Iterative Dose Reduction Three-Dimensional. PLoS ONE, 2015, 10, e0117116.	2.5	1
63	DINs: Deep Interactive Networks for Neurofibroma Segmentation in Neurofibromatosis Type 1 on Whole-Body MRI. IEEE Journal of Biomedical and Health Informatics, 2021, PP, 1-1.	6.3	1
64	Dual-Energy Computed Tomography Virtual Noncalcium Imaging for the Detection of Acute Bone Marrow Edema in Vertebrae: Qualitative and Quantitative Analysis. Journal of Medical Imaging and Health Informatics, 2021, 11, 752-759.	0.3	1
65	Dual-Energy Electronic Cleansing for Artifact-Free Visualization of the Colon in Fecal-Tagging CT Colonography. Lecture Notes in Computer Science, 2012, , 8-17.	1.3	1
66	Piecewise Structural Diffusion Defined on Shape Index for Noise Reduction in Dual-Energy CT Images. Lecture Notes in Computer Science, 2012, , 88-96.	1.3	1
67	Estimation of Necrosis Volumes in Focal Liver Lesions Based on Multi-phase Hepatic CT Images. Lecture Notes in Computer Science, 2011, , 60-67.	1.3	1
68	Dynamic-thresholding level set: a novel computer-aided volumetry method for liver tumors in hepatic CT images. , 2007, , .		0
69	Analysis of scalability of high-performance 3D image processing platform for virtual colonoscopy. , 2014, 9039, 90390U.		0
70	Imaging of the Porta Hepatis: Spectrum of Disease. Radiographics, 2014, 34, 848-848.	3.3	0
71	NIMG-64. NOVEL METHODS FOR GENOTYPE-PHENOTYPE CORRELATION IN SCHWANNOMATOSIS. Neuro-Oncology, 2016, 18, vi138-vi138.	1.2	0
72	Evaluating Glenoid Bone Loss with MRI-Generated 3-Dimensional Reconstructions. Arthroscopy - Journal of Arthroscopic and Related Surgery, 2018, 34, e30-e31.	2.7	0

#	Article	IF	CITATIONS
73	NIMG-66. LONG-TERM FOLLOW-UP OF NEUROFIBROMATOSIS TYPE 1 PATIENTS USING WHOLE-BODY MRI DEMONSTRATES DYNAMIC CHANGES IN INTERNAL NEUROFIBROMA SIZE. Neuro-Oncology, 2019, 21, vi176-vi176.	1.2	0
74	NIMC-07. LONG-TERM FOLLOW-UP OF SCHWANNOMA GROWTH BEHAVIOR IN ADULT NEUROFIBROMATOSIS TYPE 2 AND SCHWANNOMATOSIS PATIENTS USING WHOLE-BODY MRI. Neuro-Oncology, 2020, 22, ii148-ii148.	1.2	0
75	Deep-Cleansing: Deep-Learning Based Electronic Cleansing in Dual-Energy CT Colonography. Lecture Notes in Computer Science, 2021, , 43-53.	1.3	0
76	Relationship between whole-body tumor burden and quality of life in patients with neurofibromatosis Journal of Clinical Oncology, 2012, 30, 6136-6136.	1.6	0
77	NIMG-08. A MULTI-CENTER RADIOMICS-BASED MODEL TO DIFFERENTIATE BETWEEN NEUROFIBROMATOSIS TYPE 1-ASSOCIATED PLEXIFORM NEUROFIBROMAS AND MALIGNANT PERIPHERAL NERVE SHEATH TUMORS. Neuro-Oncology, 2021, 23, vi128-vi129.	1.2	0
78	Exploring the Interobserver Agreement in Computer-Aided Radiologic Tumor Measurement and Evaluation of Tumor Response. Frontiers in Oncology, 2021, 11, 691638.	2.8	0
79	Change in Humeral Anchor Position Significantly Affects Isometry in UCL Repair: A 3-Dimensional Computer Modeling Study, Journal of Shoulder and Elbow Surgery, 2022	2.6	0